Linear stability analysis of turbulent swirling combustor flows: impact of flow field and flame shapes on the PVC

Kilian Oberleithner[1]*, Michael Stöhr[2], Seong Ho Im [2], Christian Oliver Paschereit[1]

[1] Institut für Strömungsmechanik und Technische Akustik
Müller-Breslau Straße 8, 10623 Berlin, Germany
[2] German Aerospace Center (DLR), Institute of Combustion Technology
Pfaffenwaldring 38-40, 70569 Stuttgart, Germany

Abstract Swirling jets are widely used in modern lean-premixed combustors to achieve flame stabilization and improved mixing. These flows feature self-excited flow oscillations that manifest in a precessing vortex core (PVC) and helical large-scale coherent structures. In this conference contribution, we outline the general concept of local and global hydrodynamic stability analysis of turbulent flows with swirl and combustion. We apply the method to the flow and density field measured in the swirl combustor at the DLR Stuttgart. The computed eigenmodes match very well with the measured PVC frequency and correctly predict the marginal instability of the PVC limit-cycle state. Moreover, the analysis provides insights into the region where the PVC is generated and how it is suppressed by combustion.

Introduction

Swirling jets undergoing vortex breakdown are widely used for efficient lean combustion in gas turbines. Figure 1 shows a crossectional cut through the mean flow field inside a swirl-stabilized combustor. The contours, referring to velocity magnitude, indicate the annular swirling jet entering the chamber from below. The swirl-induced low pressure along the jet centerline creates a large inner recirculation zone (IRZ), and the area jump at the combustor inlet creates the outer recirculation zone (ORZ). The flame typically stabilizes in the inner shear layer that forms between the IRZ and the jet.

Although, the free-standing IRZ allows for an elegant way of flame stabilization, it triggers large-scale synchronized flow oscillations that may significantly affect the combustion performance. The IRZ allows for the upstream propagation of flow instabilities that resonate with the incoming perturbations leading to a global flow instability. These global instabilities are characterized by a single oscillatory frequency and a characteristic mode shape. For the swirling jet, this mode is typically spiral-shaped rotating with the base flow [1, 2, 3]. It features a so-called precessing vortex core (PVC) near the combustor inlet and large-scale helical vortices in the inner and outer shear layers. These intrinsic flow dynamics significantly affect the flame dynamics and mixing characteristics[4, 5, 6].

In recent years, significant improvement was achieved in describing these flow oscillations by means of hydrodynamic linear stability analysis. The concept of local and global stability theory that is well established for low Reynolds number laminar base flows [7, 8], was carried over to high Reynolds number turbulent flows with and without combustion [9, 3, 10, 11]. In contrast to the classic (laminar) approach, the analysis is based on the time-averaged turbulent flow field and the large-scale coherent flow structures are related to the mean flow eigenmodes. Such an analysis becomes inherently nonlinear as the mean flow itself is formed nonlinearly by the turbulent and coherent Reynolds stresses. It therefore allows for prediction of the nonlinerely saturated limit-cycle and may deal as an analytic post-processing tool of experimental or numerical data[12, 13, 9, 14]. Dealing with mean flow data, the analysis may not necessarily reveal the onset of the instability, but it accurately describes the driver of the limit-cycle. The analysis may tell where in the flow field the resonance occurs and, consequently, how it can be suppressed through mean flow modifications.

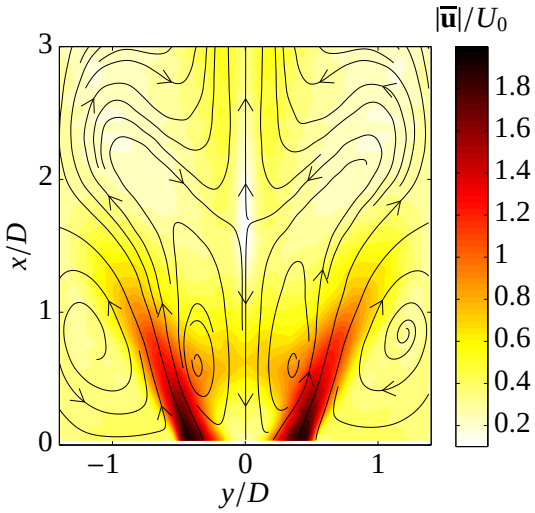

Figure 1: Mean flow field of a swirl-stabilized combustor (isothermal). The flow enters the chamber from the bottom.

In this article we report on a recent collaborative work of the TU Berlin and the DLR Stuttgart. Experimental observations at the DLR Stuttgart have shown that the

*Corresponding author: oberleithner@tu-berlin.de

PVC only occurs for combustion conditions that feature a detached M-shaped flame. This suggests that the flame shape and associated temperature field affects the formation of the PVC. Similar observations were conducted in a different facility at the TU Berlin and others [15, 11]. The aim of this study is to understand how the flame influences the formation of the PVC and *vice versa*.

In the following, we explain the main steps for a hydrodynamic linear stability analysis of turbulent flows with swirl and combustion. We demonstrate the method on the mean flow and density fields obtained from measurements conducted at the DLR Stuttgart. Eddy viscosity models that account for the interaction of the coherent structure with the background turbulence are deduced from the experimental data and implemented into the stability solver. We implement a local stability approach where the flow field is considered as locally parallel. In contrast to the more rigorous global stability analysis, this approach is less sensitive to the choice of the boundary conditions. As will be shown in this article, linear stability analysis provides insights into fundamental mechanisms that are not given by experimental data. We hope that this article will motivate other researchers to analyze their experimentally or numerically derived turbulent mean flows.

Stability equations for turbulent flows

We start off with the classic triple decomposition of the turbulent flow data. The instantaneous flow field vector $\mathbf{u}(\mathbf{x}, t)$ is decomposed into a time-averaged part $\overline{\mathbf{u}}(\mathbf{x})$, a periodic (coherent) part $\tilde{\mathbf{u}}(\mathbf{x}, t)$, and a randomly fluctuating (turbulent) part $\mathbf{u}''(\mathbf{x}, t)$, reading

$$\mathbf{u}(\mathbf{x}, t) = \overline{\mathbf{u}}(\mathbf{x}) + \tilde{\mathbf{u}}(\mathbf{x}, t) + \mathbf{u}''(\mathbf{x}, t). \tag{1}$$

The phase-average $\langle \mathbf{u}(\mathbf{x}, t) \rangle$ is used to separate the fine-scale turbulent fluctuations from the coherent motion such that $\tilde{\mathbf{u}}(\mathbf{x}, t) = \langle \mathbf{u}(\mathbf{x}, t) \rangle - \overline{\mathbf{u}}(\mathbf{x})$.

The triple decomposition is substituted into the incompressible Navier–Stokes equation and the continuity equation, and, after some manipulations, the governing equations for each of the three parts can be formulated [16]. The mean flow equations are

$$\overline{\mathbf{u}} \cdot \nabla \overline{\mathbf{u}} = -\frac{1}{\rho} \nabla \overline{p} + \frac{1}{\mathrm{Re}} \nabla^2 \overline{\mathbf{u}} - \nabla \cdot \left(\overline{\mathbf{u}'' \mathbf{u}''} + \overline{\tilde{\mathbf{u}} \tilde{\mathbf{u}}} \right) \tag{2a}$$

$$\nabla \cdot \overline{\mathbf{u}} = 0, \tag{2b}$$

indicating how the mean flow is modified through the generation of turbulent and coherent Reynolds stresses. The equations for the coherent motion are given as

$$\frac{\partial \tilde{\mathbf{u}}}{\partial t} + \tilde{\mathbf{u}} \cdot \nabla \overline{\mathbf{u}} + \overline{\mathbf{u}} \cdot \nabla \tilde{\mathbf{u}} = -\frac{1}{\rho} \nabla \tilde{p} + \frac{1}{\mathrm{Re}} \nabla^2 \tilde{\mathbf{u}} - \nabla \cdot \left(\tau^N + \tilde{\tau} \right) \tag{3a}$$

$$\nabla \cdot \tilde{\mathbf{u}} = 0, \tag{3b}$$

where the nonlinear terms $\tau^N = \tilde{\mathbf{u}} \tilde{\mathbf{u}} - \overline{\tilde{\mathbf{u}} \tilde{\mathbf{u}}}$ are neglected in the following. The terms $\tilde{\tau} = \langle \mathbf{u}'' \mathbf{u}'' \rangle - \overline{\mathbf{u}'' \mathbf{u}''} = \widetilde{\mathbf{u}'' \mathbf{u}''}$ represent the modification of the turbulent field during the passage of a coherent structure. These turbulent-coherent interactions are unknown and must be modeled appropriately. The mean-coherent and mean-turbulent interactions are reflected in the actual mean flow shape and are implicitly accounted for in the perturbation equations (3).

Calculation of eddy viscosity

The turbulent-coherent interactions are modeled through a Newtonian eddy viscosity model

$$\tilde{\tau}_{ij} = -\widetilde{u_i'' u_j''} = \nu_t \left(\frac{\partial \tilde{u}_i}{\partial x_j} + \frac{\partial \tilde{u}_j}{\partial x_i} \right), \tag{4}$$

where ν_t is the eddy viscosity of the undisturbed flow and the indices $i, j = 1, 2, 3$ indicate the three velocity components. In swirling flows, several Reynolds stress components are relevant and the eddy viscosity is approximated through a least-square fit over all resolved Reynolds stresses [17], yielding

$$\nu_t = \frac{\left(-\overline{u_i'' u_j''} + \frac{2}{3} k \delta_{ij} \right) \cdot \left(\frac{\partial \overline{u}_j}{\partial x_i} + \frac{\partial \overline{u}_i}{\partial x_j} \right)}{\left(\frac{\partial \overline{u}_k}{\partial x_l} + \frac{\partial \overline{u}_l}{\partial x_k} \right) \cdot \left(\frac{\partial \overline{u}_k}{\partial x_l} + \frac{\partial \overline{u}_l}{\partial x_k} \right)} \tag{5}$$

with the summation over the repeating indices i, j, k, and $l = 1, 2, 3$.

Solving for global modes

Equation (3) is solved for a (global) perturbation having the form

$$\tilde{\mathbf{u}}(\mathbf{x}, t) = \hat{\mathbf{u}}(\mathbf{x}) \mathrm{e}^{-i \omega_g t} + c.c. \tag{6}$$

with the complex three-dimensional shape function $\hat{\mathbf{u}}$ and the complex global mode frequency $\omega_g = \omega_{g,r} + i \omega_{g,i}$. The global mode growth rate and frequency is determined by the real and imaginary part of ω_g, and the entire flow field is said to be globally unstable if $\omega_{g,i} > 0$.

Mean flow versus base flow analysis

For the derivation of the perturbation equations (3), it is assume that the base flow $\overline{\mathbf{u}}$ is a steady solution of the governing equations. In the present work, we relax this assumption and assign $\overline{\mathbf{u}}$ to the time-averaged flow, which is a steady solution of the forced Navier–Stokes equations[13].

The analysis of the mean flow introduces a conceptional difference to the analysis of the base flow. This is explained in the Fig. 2. It illustrates the limit-cycle amplitude A_{sat}, the global mode growth rate $\omega_{g,i}$, and the global mode frequency $\omega_{g,r}$, for a flow that undergoes a supercritical Hopf bifurcation. Think the control parameter P as the Reynolds number for the cylinder wake or the swirl number for the swirling jet. Approaching the critical point from subcritical conditions ($P < P_{\mathrm{crit}}$), the flow remains steady ($|A_{\mathrm{sat}}| = 0$) and globally stable with a negative global mode growth rate. At the critical point, the

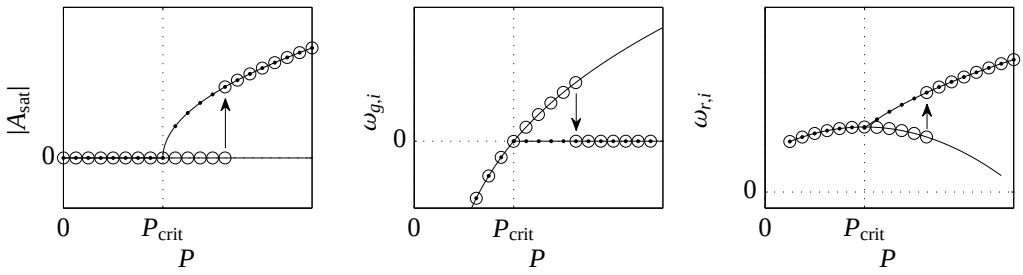

Figure 2: Conceptual drawing of a supercritical Hopf bifurcation; Oscillation amplitude (a), linear global mode growth rate (b) and frequency (c) versus control parameter P. The black line refers to the base flow solution and the black lines with dots to the limit-cycle. The black circles mark the bifurcation from the unstable steady to the stable unsteady solution at supercritical conditions.

flow becomes marginally unstable ($\omega_i = 0$). By exceeding the critical point, the base flow solution becomes linearly unstable ($\omega_i > 0$). At these supercritical conditions, any small perturbation will initiate the global mode. It will first grow exponentially at the rate given by the base flow stability and then saturate at the limit-cycle. The saturation of the global mode is a nonlinear process that manifests in the generation of Reynolds stresses, which in turn modify the mean flow. The stability analysis of the corrected mean flow is thus, inherently nonlinear, taking these saturation processes into account. The limit-cycle is represented by a marginally stable global mode with the global mode frequency to coincide with the oscillation frequency. The validity of the mean field analysis has been demonstrated for the cylinder wake[13, 18, 12], for the swirling jet [3], and for the oscillating non-swirling jet [14].

Weakly nonparallel flow approximation

Introducing (6) into (3) leads to a stability eigenvalue problem, which can easily reach impractical size [19]. To reduce the numerical effort, the stability problem (3) is first solved locally and the global stability properties are thereafter deduced from the local stability properties. The same approach has recently been adopted in several related studies dealing with swirling and non-swirling wake flows [12, 3, 9, 10, 20, 21, 22]. A local eigenvalue problem is posed by adopting a quasi parallel, axially symmetric velocity profile

$$\overline{\mathbf{u}}(r) = (u_x(r), 0, u_\theta(r))^T, \tag{7}$$

where u_x and u_θ are the axial and azimuthal velocity component, respectively. In a parallel flow, the radial component $u_r(r)$ is set to zero to satisfy the continuity equation. For the parallel flow, the perturbation

$$\tilde{\mathbf{u}}(\mathbf{x}, t) = \hat{\mathbf{u}}(r)\mathrm{e}^{i(\alpha x + m\theta - \omega t)} + c.c. \tag{8}$$

is homogeneous in the streamwise and azimuthal directions. Here α denotes the complex streamwise wavenumber, ω the complex frequency, and m the real azimuthal wavenumber. In this work we solve for the $m = 1$ mode, which corresponds to a single-helical instability.

The local stability is linked to the global stability through the concept of convective and absolute instability and the determination of the global mode wavemaker [7, 8]. A convective instability is swept away from its source leaving the flow ultimately unperturbed. An absolute instability grows in the upstream and downstream directions, ultimately perturbing the entire parallel flow. The convective/absolute instability is determined through the impulse response to a localized perturbation. If the resulting wavepacket spreads in the upstream and downstream directions, the parallel flow is considered as absolutely unstable. For large times, the impulse response is determined by the wave at zero group velocity $\partial\omega/\partial\alpha = 0$, which is the necessary condition for a saddle point in the complex alpha plane. The complex frequency at this saddle point is called the absolute frequency $\omega_0 = \omega_r + i\omega_i$. The flow profile is absolutely unstable if $\omega_{0,i} > 0$ and absolutely stable if $\omega_{0,i} < 0$. In this work, the absolute frequency is determined for each streamwise location using a so-called spatio-temporal analysis where the local eigenvalue problem is solved for complex ω and complex α. The saddle point in the α plane is determined by minimizing the functional $F = (\partial\omega_i/\partial\alpha_r)^2 + (\partial\omega_i/\partial\alpha_i)^2$. Details of the numeric scheme are given in [23, 10].

Once the absolute frequency is computed for the profiles at each streamwise station, the global stability is derived from the resulting streamwise distribution of ω_0. The local and global stability are connected through the concept of the global mode wavemaker [24, 25]. At the streamwise location of the wavemaker, the global mode frequency and growth rate is equal to the local absolute growth rate. There are two criteria that define the position of the wavemaker [7, 8].

1. *The region of absolute instability is nested in a region of convective instability*:
   The global mode frequency is then given by the saddle point criterion

   $$\omega_g = \omega_0(x_s) \quad \text{with} \quad \frac{\mathrm{d}\omega_0}{\mathrm{d}x}(x_s) = 0, \tag{9}$$

   which involves an analytical continuation of $\omega_0(x)$ in the complex x plane. The streamwise location x_s determines the location of the global mode

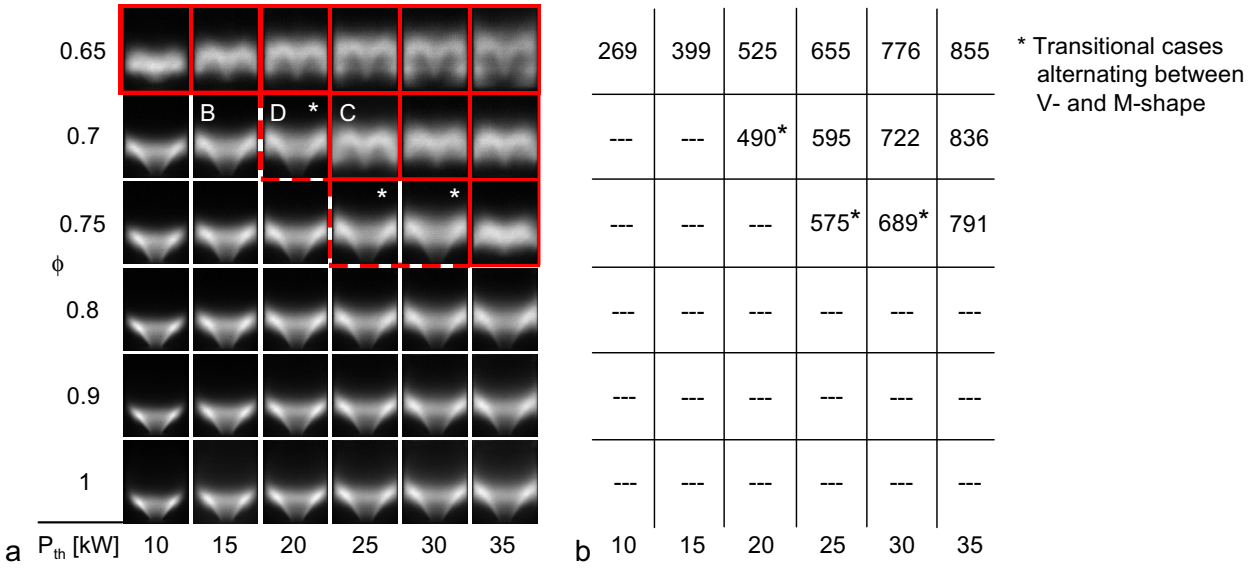

Figure 3: (a) Flame shapes for different values of thermal power P_{th} and equivalence ratio ϕ. The conditions where a PVC occurs are marked red. (b) Precession frequencies of the PVC detected in the acoustic spectrum.

wavemaker where the global mode frequency $\omega_{g,r}$ and growth rate $\omega_{g,i}$ is determined.

2. *The region of absolute instability is attached or close to the flow inlet*:
   The wavemaker is located at the inlet and the global mode frequency and growth rate is equal to the absolute frequency at the inlet

$$\omega_g = \omega_0(x = 0) \quad \text{and} \quad x_s = 0. \tag{10}$$

The first criterion applies to the Kármán vortex street [12] and swirling jets with a detached vortex breakdown bubble [26, 10, 11]. The second criterion applies to swirling jets with the vortex breakdown bubble attached to the inlet.

Experimental observations

Experimental studies were performed in a gas turbine model combustor derived from an industrial design by Turbomeca, which can be operated in a partially premixed [27, 28] and a perfectly premixed [29] configuration. In this work, the combustor is operated at atmospheric pressure with perfectly premixed methane and air.

Flames were characterized using OH-CL imaging and pressure recording for thermal power P_{th} ranging between 10 and 35 kW and equivalence ratios ϕ between 0.65 and 1. The OH-CL images, which are considered as a marker of the flame zone [30], are shown in Fig. 3a. The images show two main types of flame shape, namely the M-shaped flame type (conditions marked with the red envelope) and the V-shaped type in the remaining range of conditions. While the V-shaped flames are generally attached to the burner nozzle, the base of the M-shaped flames is lifted approximately 10 mm above the nozzle. There are also three transitional cases (marked with an asterisk), where the flame alternates randomly between V- and M-shape (the typical time between shape-changes is on the order of 1 s). One of these transitional, bi-stable flames (case D) is studied in more detail in an accompanying work [31].

The occurrence of a PVC was detected using the power spectrum of the pressure difference signal. If present, the PVC exhibits a characteristic peak at its precession frequency f_{PVC}. For the cases where a PVC was observed, the values of f_{PVC} are specified in the table shown in Fig. 3b. Comparing the occurrence of the PVC listed in Fig. 3b with the flame shapes in Fig. 3a reveals that a PVC always occurs for the M-shaped flames, whereas the V-shaped flames generally do not exhibit a PVC. For the three transitional cases (marked with an asterisk), the PVC appears in the acoustic spectrum only during the periods when the flame is in M-shape. Non-reacting conditions have been measured in a previous work by Steinberg et al. [29] for thermal powers in the range P_{th}=10-35 kW, and for all cases a PVC was found.

Stability analysis of the reacting flow

Figure 4 shows the results of the stability analysis of the attached (case B) and detached (case C) flame. Computations are conducted with and without taking the density field into account. For the attached flame, which features no PVC, the absolute growth rate is significantly decreased when taking the density field into consideration. Particularly at the inlet, where the density stratification is strong, the growth rate is significantly reduced. The comparison between the isothermal and stratified computations reveal that the flow field itself is globally unstable with the wavemaker located at the inlet, and the non-existence of the PVC is only reproduced if the density field is taken into consideration. This strongly suggests that the PVC that exists at isothermal conditions is

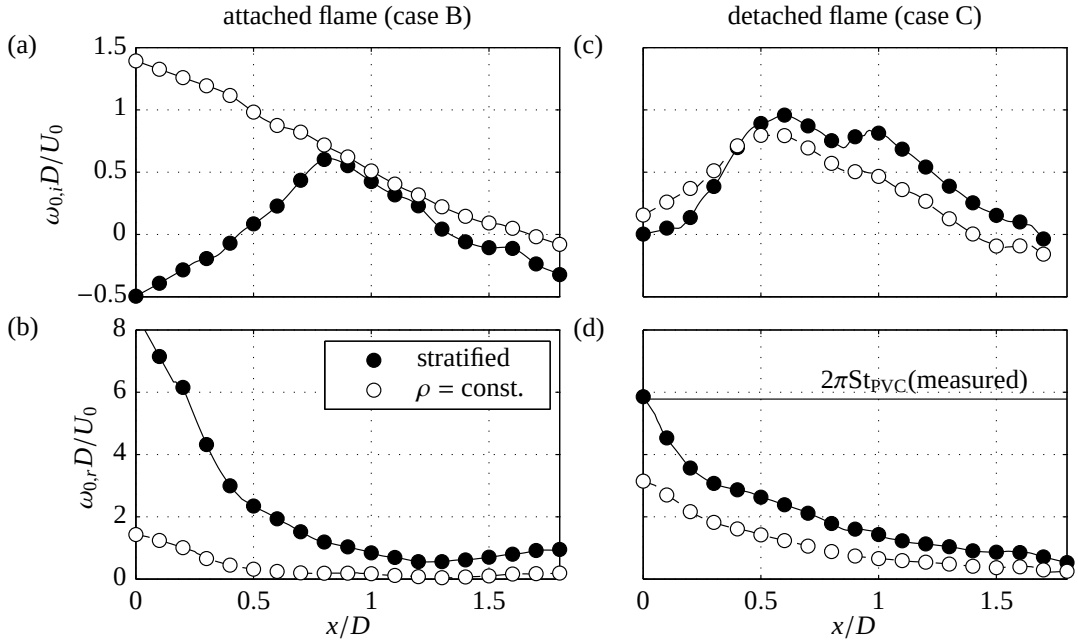

Figure 4: Reacting flow: absolute growth rate (a-b) and frequency (c-d) derived from the linear stability analysis for case B (a,c) and case C (b,d). Computations are conducted for the reacting flows assuming a homogeneous density field and with the actually measured density field. For case B the PVC instability at the inlet is suppressed by the density field.

suppressed by the density stratification in the inlet region induced by the attached flame.

For the detached flame in case C, the influence of the density field on the flow stability is less significant. The stability analysis of the stratified flow reveals a semifinite region of absolute instability (Fig. 4c). The wavemaker is located at the inlet with the global mode frequency $\omega_g = \omega_0(x = 0)$. The resulting global mode oscillation frequency f=$\omega_{g,r}/2\pi$=603 Hz agrees well with the measured PVC frequency of 595 Hz (cf. Fig. 4d), and the marginal instability $\omega_{g,i} \approx 0$ is confirmed. By neglecting the density stratification for case C, the absolute growth rate at the inlet is predicted somewhat too high, while the PVC frequency is predicted much too low. The analysis reveals that the density stratification in case C does not affect the global mode growth rate, but it significantly alters the oscillation frequency. Since the radial density gradients are small in between the IRZ and the annular jet, the effect on the PVC frequency must be caused by the density differences between the ORZ and the annular jet.

The linear stability analysis of the reacting cases B and C has shown that the mean flow and density field determines the occurrence or absence of the PVC. The PVC in turn, however, influences the flame shape and thereby the flow and density field. The question whether a flame with or without PVC will form at a certain condition thus depends on a complex unsteady interplay of flame propagation and the flow/density field. This interplay is further examined in an accompanying work [31], which studies a bi-stable condition (case D in Fig. 3) where the flame alternates randomly between V- and M-shape, and thus, the PVC is repeatedly formed and suppressed.

Conclusions

The present work studies the formation and flame-induced suppression of self-excited flow oscillations in a GT-typical swirl combustor. The oscillations manifest in the precession of the vortex core (PVC) and the synchronized roll-up of large-scale helical coherent flow structures. Several previous studies have shown a significant impact of the PVC on the dynamics and shape of turbulent swirl flames [5, 6, 32].

The work follows up a recently established approach, where the PVC is identified as the manifestation of a self-excited global hydrodynamic instability [9, 10, 11]. Utilizing a local linear stability analysis (LSA), the frequency, wavemaker, and shape of this instability is predicted theoretically and compared to experimental data.

The stability analysis of the time-averaged flow successfully identifies the PVC as a global mode and reveals the importance of the fluid density in the wavemaker region. The present work demonstrates that the stability analysis of experimental mean flow data is a valuable post-processing tool to reveal the mechanisms that lead to flow oscillations. The local analysis outlined here can be applied to a wide range of complex flow configurations.

Acknowledgments

The authors kindly acknowledge the financial support of the German Research Foundation (DFG), the Research Association for Combustion Engines (FVV), and

the DLR project IVTAS.

References

[1] H. Liang, T. Maxworthy, J. Fluid Mech. 525 (2005) 115–159.

[2] M. R. Ruith, P. Chen, E. Meiburg, T. Maxworthy, J. Fluid Mech. 486 (2003) 331–378.

[3] K. Oberleithner, M. Sieber, C. N. Nayeri, C. O. Paschereit, C. Petz, H.-C. Hege, B. R. Noack, I. Wygnanski, J. Fluid Mech. 679 (2011) 383–414.

[4] N. Syred, Prog. Energy Combust. Sci. 32 (2006) 93 – 161.

[5] M. Stöhr, R. Sadanandan, W. Meier, Exp. Fluids 51 (2011) 1153–1167. 10.1007/s00348-011-1134-y.

[6] M. Stöhr, I. Boxx, C. D. Carter, W. Meier, Combust Flame 159 (2012) 26362649.

[7] P. Huerre, P. A. Monkewitz, Annu Rev Fluid Mech 22 (1990) 473–537.

[8] J.-M. Chomaz, Annu. Rev. Fluid Mech. 37 (2005) 357–392.

[9] M. P. Juniper, in: ASME Turbo Expo 2012: Turbine Technical Conference and Exposition, GT2012-68253, American Society of Mechanical Engineers, pp. 189–198.

[10] K. Oberleithner, S. Terhaar, L. Rukes, C. O. Paschereit, in: Proceedings of ASME Turbo Expo 2013, ASME paper GT2013-95509.

[11] S. Terhaar, K. Oberleithner, C. Paschereit, Proceedings of the Combustion Institute 35 (2015) 3347 – 3354.

[12] B. Pier, J Fluid Mech 458 (2002) 407–417.

[13] D. Barkley, Europhys Lett 75 (2006) 750–756.

[14] K. Oberleithner, L. Rukes, J. Soria, J. Fluid Mech. 757 (2014) 1–32.

[15] S. Terhaar, K. Oberleithner, C. O. Paschereit, Combust Sci Technol 186 (2014).

[16] W. C. Reynolds, A. K. M. F. Hussain, J Fluid Mech 54 (1972) 263–288.

[17] E. M. Ivanova, B. E. Noll, M. Aigner, J. Eng. Gas Turb. Power 135 (2013) 011505.

[18] B. R. Noack, K. Afanasiev, M. Morzyński, G. Tadmor, F. Thiele, J Fluid Mech 497 (2003) 335–363.

[19] V. Theofilis, Annu. Rev. Fluid Mech. 43 (2011) 319–352.

[20] K. Oberleithner, C. O. Paschereit, I. Wygnanski, J Fluid Mech 741 (2014) 156–199.

[21] U. A. Qadri, D. Mistry, M. P. Juniper, J Fluid Mech 720 (2013) 558–581.

[22] M. P. Juniper, B. Pier, European Journal of Mechanics - B/Fluids (2014) –.

[23] M. P. Juniper, O. Tammisola, F. Lundell, J. Fluid Mech. 686 (2011) 218–238.

[24] J. M. Chomaz, P. Huerre, L. G. Redekopp, Phys. Rev. Lett. 60 (1988) 25–28.

[25] P. A. Monkewitz, P. Huerre, J.-M. Chomaz, J. Fluid Mech. 251 (1993) 1–20.

[26] F. Gallaire, M. Ruith, E. Meiburg, J.-M. Chomaz, P. Huerre, J Fluid Mech 549 (2006) 71–80.

[27] W. Meier, P. Weigand, X. Duan, R. Giezendanner-Thoben, Combust. Flame 150 (2007) 2–26.

[28] P. Weigand, W. Meier, X. Duan, M. Aigner, J. Eng. Gas Turb. Power 129 (2007) 664–671.

[29] A. M. Steinberg, C. M. Arndt, W. Meier, Proc. Combust. Inst. 34 (2013) 3117–3125.

[30] Y. Hardalupas, M. Orain, Combust. Flame 139 (2004) 188–207.

[31] M. Stöhr, K. Oberleithner, C. M. Arndt, A. M. Steinberg, W. Meier, in: Proceedings of the 7th European Combustion Meeting (2015), Budapest, Hungary.

[32] M. Stöhr, C. Arndt, W. Meier, Proc. Combust. Inst. 34 (2013) 3107–3115.